Monte Carlo Simulations of the Phase Behavior of Surfactant Solutions

R. Larson

Monte Carlo Simulations of the Phase Behavior of Surfactant Solutions

R.G. Larson (*)

Bell Laboratories, Lucent Technologies, 700 Mountain Avenue, Murray Hill, NJ 07974, USA

(Received 19 March 1996, revised 10 June 1996, accepted 2 July 1996)

PACS.61.20.Gy – Theory and models of liquid structure
PACS.61.20.Ja – Computer simulation of liquid structure
PACS.64.70.Md – Transitions in liquid crystals

Abstract. — Phase diagrams are determined by Monte Carlo lattice simulations for idealized symmetric and asymmetric surfactant molecules mixed with single-site "oil" and "water" molecules. At high concentrations (above 20%) of surfactant, the simulations show the self assembly of liquid crystalline phases, including smectic, hexagonal, BCC sphere packings, and Ia3d gyroid cubic phases. The locations of the phases on the diagram for asymmetric surfactants in "water" are shifted relative to those for a symmetric one in a way that favors phases whose surfactant-laden interfaces curve so that the bulkier group is on the convex side of the interface. When the system composition is gradually changed, cylinders of a hexagonal phase are oriented along the 111 direction of the micellar BCC or Ia3d phase into which the cylinders epitaxially transform, with the d-spacing ratios of 1.22 and 2.12, respectively. These and many other aspects of the predicted phase behavior, including the compositions at which transitions among ordered phases occur, compare favorably with experimental observations for nonionic, cationic, anionic, and zwitterionic single-tail surfactants.

1. Introduction

The phase diagrams of surfactants or lipids mixed with water and/or oil show both universal and particular features. Many of the same phases are recurrent in widely disparate systems, including lamellar, hexagonal cylindrical, disordered micellar, and intermediate [1–6]. However, other aspects of the phase behavior are sensitive to amphiphile type, temperature, and the presence and amounts of solvents, co-surfactants, and salts. Figure 1 illustrates some "universal", as well as "non-universal", aspects of the phase behavior in water of four disparate single-tailed surfactants: a nonionic, an anionic, a cationic, and a zwitterionic surfactant. In each case, there are, with increasing surfactant concentration, transitions from a disordered solution of spherical micelles to a hexagonal packing of cylinders (H), then to an intermediate phase (G; except in (b); see below), and finally to a lamellar phase (L_α). Similar behavior is observed in aqueous solutions of other single-tailed surfactants [7–9]. In each case in Figure 1, the order-disorder transition on heating or cooling occurs at the highest temperature for the lamellar phase, the next highest temperature for the hexagonal phase, and at lower temperatures for the other phases. Note also that the order-order transitions in each case are largely

(*) e-mail: rgl@likewise.att.com

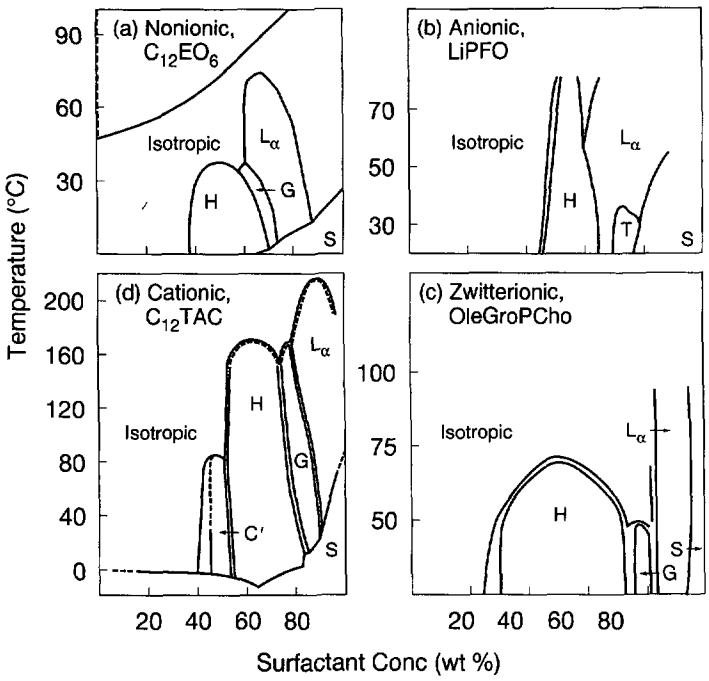

Fig. 1. — Phase diagrams of four surfactants in water. "H" and "L_α", stand for hexagonal and lamellar phases, "G" and "T" are gyroid cubic and tetragonal mesh intermediate phases, "C'" is a cubic packing of spherical micelles, and "S" stands for crystalline solid. (a) hexa-ethyleneglycol mono n-dodecyl ether, $C_{12}EO_6$ (from Clerc *et al.* [4]), (b) lithium perfluorooctanoate. LiPFO (from Kekicheff and Tiddy, 1989), (c) 1-oleoyl-sn-glycero-3-phosphocholine. OleGroPCho (from Arvidson *et al.* [2]), and (d) dodecyltrimethylammonium chloride $C_{12}TAC$ (from Balmbra *et al.* [1]).

lyotropic — that is, they are driven mainly by changes in concentration, not temperature. These similarities among the phase diagrams for different surfactant molecules suggest that the phase transitions are driven mainly by "universal" features of surfactant mixtures, such as volume-filling constraints, entropies and energies of mixing, and entropies of surfactant chain conformation.

However, there are also some differences among the phase diagrams of Figure 1. For one surfactant (the cationic), there is a cubic phase wedged between the hexagonal cylinders and the disordered spheres; this is almost certainly a cubic packing of spheres. In addition, the particular intermediate phase that forms varies from one surfactant to the next. For example, a "mesh" phase ("T" phase), consisting of tetragonally ordered holes perforating lamellar sheets, forms at low temperatures in the system containing the anionic perfluorooctanoate surfactant, while cubic Ia3d intermediate phases, called "gyroid" (G) phases, are formed by the other three surfactants in Figure 1. Also, the order-order transition compositions vary from one surfactant to the next. In Figure 1, for example, the lamellar compositional window shifts to the right as one moves in the clockwise progression from a) to d). A similar shift occurs in the hexagonal window of compositions, except that this window is enlarged for the zwitterionic surfactant, Figure 1c.

Divergences from the phase behavior typified by Figure 1 can be found in aqueous solutions of one- or two-tailed lipids [5,6], for which the tail groups are especially bulky. Example phase

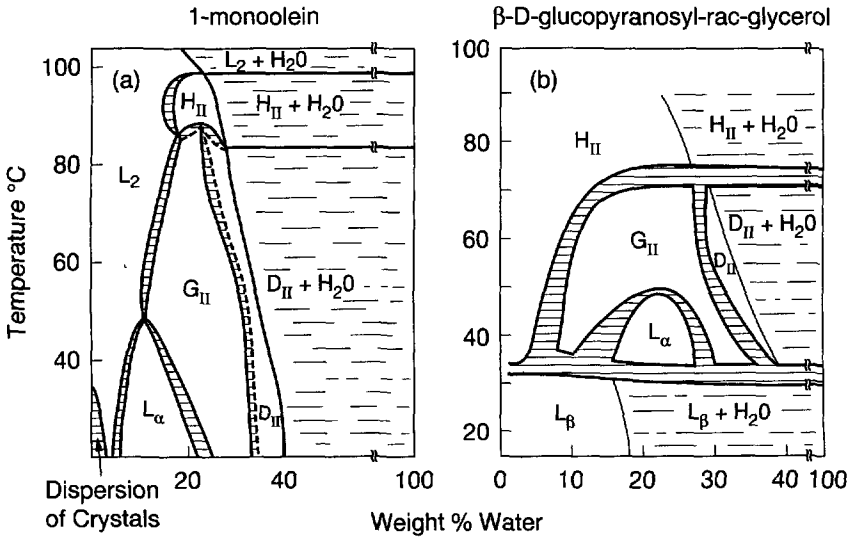

Fig. 2. — Phase diagrams for (a) 1-monoolein in water (from Larsson [5]), and (b) di-dodecyl alkyl-β-D-glucopyranosyl-rac-glycerol (from Turner *et al.* [6]) in water. "H_{II}" is the inverse hexagonal phase, G_{II} is the inverse gyroid Ia3d, and "D_{II}" is the inverse double-diamond Pn3m phase. In the inverse phases, the aqueous phase is inside the channels.

diagrams for 1-monoolein [5] and for di-dodecyl alkyl-β-D-glucopyranosyl-rac-glycerol [6] are shown in Figure 2. These are dominated by inverse phases, namely an inverse Ia3d (G_{II}), an inverse Pn3m "double-diamond" (D_{II}) cubic phase, and an inverse hexagonal phase (H_{II}).

A pattern of universality and particularity also prevails in the phase behavior of *diblock copolymers*. Diblock copolymers are polymeric amphiphiles consisting of two chemically distinct linear polymer chains, with one end of one chain covalently bonded to one end of the other. These also show a progression from disordered spheres to cubically ordered spheres to hexagonal cylinders to lamellar phases when a composition variable, such as the ratio of the block lengths, or the concentration of added homopolymer, is varied [10, 11]. Diblock copolymer phase diagrams also have "nonuniversal" features; in particular, the intermediate phase between hexagonal and lamellar can be either a "mesh" phase with rhombohedral symmetry, or a cubic phase, with Ia3d symmetry [12–15]. As with surfactants, the locations on the phase diagram of the ordered phases can vary somewhat, depending on the molecular structure.

In this paper, we seek to understand some of the sources of universality and non-universality in the phase diagrams of such surfactant and block copolymer systems by using a simple Monte Carlo lattice model, one which contains only the most basic features of amphiphilic systems [16–18]. These basic features are the near-neighbor relative repulsion between unlike chemical moieties, the configurational entropy of the chain-like surfactant (or block-copolymer) molecules, the entropies of mixing, and the excluded-volume or space-filling requirements of condensed states of matter. Since these physical features are universal, we believe that the phase behavior predicted by this simple model can be regarded as a prototype against which the behavior of real systems can be compared. Such comparisons will help distinguish the characteristics of the real systems that are due to the basic features of surfactants described above from those that have their origins in the particularities of these real systems, such as the details of molecular shapes, molecular stiffness, ionic effects, hydrogen bonding, *etc.* Although the model we introduce has one peculiarity of its own, namely its underlying lattice, we have

shown elsewhere [18] that the lattice introduces remarkably few artifacts, and can support essentially all the phases observed in these systems: disordered, lamellar, hexagonal, cubic and "mesh" intermediate phases, as well as cubic packings of spheres.

2. Lattice Model and Simulation Technique

The details of the Monte Carlo lattice model have been discussed elsewhere [16, 17]. The simulated surfactant molecule, designated H_iT_j, is a sequence of i "head" units connected to j "tail" units, each unit occupying one site on the simple cubic lattice, with periodic boundary conditions. A site on the amphiphilic chain can be connected to any of its $z = 26$ nearest or diagonally-nearest neighbors. The amphiphile is thus a sequence of $N = i + j$ units that remain attached together *via* nearest-neighbor or diagonally-nearest-neighbor bonds; Monte Carlo moves that sever an amphiphile are rejected.

The "solvent" molecules in the simulation are of two types, which we call "water" and "oil". These are taken to be chemically identical, respectively, to the "head" and "tail" units on the amphiphile chain. Each unit interacts equally strongly with all 26 nearest and diagonally-nearest neighbors. There is a single dimensionless interaction energy parameter w, which is the interaction energy per head/tail contact, divided by k_BT. For convenience, we shall refer to $1/w$ as simply the "temperature" of the system. The scale of the energetic interactions between oil and water solvent molecules is controlled by the product zw; for example $w = 0.1538$ corresponds to $zw = 4$, which is a factor of two higher at the mean-field critical point $zw = 2$ for an oil/water mixture. Thus, at $w = 0.1538$, the oil and water have a strong tendency to demix. A second relevant energy scale controls the tendency of the head and tail units of the amphiphile to micro-separate from each other; this energy scale is Nwz. For $N = 8$ and $w = 0.1538$, we obtain $Nwz = 32$, a value large enough that the amphiphile tends to form microseparated domains or liquid crystalline phases, such as smectic and hexagonal phases.

The amphiphilic molecules rearrange themselves on the lattice by "reptation" and "kink"-like motions, as discussed elsewhere [16,17]. A reptation move consists in the movement of one of the two end units of chain (say unit "1") into a solvent-occupied site. Unit "2" of the chain is then moved into the site formerly occupied by unit "1", unit "3" into the unit "2" site, *etc.* The site vacated by the last unit of the chain is taken up by the solvent unit displaced from its site by unit "1". A "kink" motion is the movement of a single chain unit into a neighboring site, with the displaced the occupant of that site moving into the site vacated by the chain unit. Moves are accepted or rejected using the usual Metropolis scheme. As in earlier work, we obtain equilibrium ordered or disordered phases on $L \times L \times L$ lattices, where L is an integer, by starting at infinite temperature ($w = 0$), and "cooling" the system by increasing w in small increments until the desired value of w is reached.

In previous work, the volume fractions of oil and water were both held fixed during the simulation; thus the Metropolis sampling was carried out within a *closed* ensemble. For simulations in the closed ensemble, one chooses the desired volume fractions of oil, water, and amphiphile. Then one equilibrates the system at "infinite temperature," *i.e.*, at $w = 0$; lowers the temperature by raising w; and re-equilibrates at this higher value of w. Further step increases in w followed by re-equilibration are then made, with increments in w usually kept below $\Delta w \leq 0.01$, until the desired value of w is reached. The equilibrated structure is then identified, by inspection, as a disordered one, or as one of the regular structures: lamellar, hexagonal, body-centered cubic micelles (BCC), or gyroid, and the size of the unit cell is identified. If the structure is lamellar, it is examined for the presence of perforations in either the water-continuous layer or the oil-continuous one.

We also find it convenient to use in some simulations a *partially open* ensemble in which oil

units can be replaced by water, and *vice versa*, during a run. These runs are carried out at a fixed chemical potential difference $\Delta\mu \equiv (\mu_0 - \mu_w)/k_BT$, between oil and water. To implement this scheme, the Metropolis algorithm is modified in an obvious way: the dimensionless energy change $\Delta E/k_BT$ resulting from an exchange of a water for an oil unit is evaluated, and added to the chemical potential difference $\Delta\mu$. If the result is negative, the move is accepted; if it is positive, it is accepted with probability $\exp(-(\Delta E/k_BT + \Delta\mu))$. In these "partially open" runs, the amphiphile concentration remains fixed, as it does in runs in the closed ensemble. Using the system configuration generated at a given value of $\Delta\mu$ as a starting state for a new run with an incrementally different value of $\Delta\mu$, the oil/water ratio and structure can then evolve away from that established during the previous run. If there is a phase transition, the new phase is identified, the chemical potential is changed again, and a new run initiated. Because the composition can be varied at fixed w in simulations with partially open systems, more rapid exploration of the phase diagram at a given w is possible than in the closed ensemble. In addition, with the partially open ensemble, we find order-order phase transitions readily occur, and the *epitaxial relationship* between the two ordered structures can be determined. Furthermore, in a partially open ensemble, the presence of multi-phase regions can sometimes be recognized by the occurrence of an abrupt change in composition resulting from a small change in $\Delta\mu$.

As discussed below, we find some *hysteresis* in the composition at which phase transitions occur; *i.e.*, the composition at which a transition occurs can depend on the direction in which $\Delta\mu$ is changed. The hysteresis can become large at low concentrations of surfactant (20% by volume or less). In such cases, simulations on the *closed* ensemble help determine more accurately the locations of phase boundaries. Run durations are around 10^5 attempted Monte Carlo moves per lattice site at low temperatures ($w \gtrsim 0.1$). Systematic drifts in the system energy averaged over the run prove to be tell-tale signs of a progressing phase transition. Whenever such drifts are detected, the runs are extended as long as necessary at fixed w to achieve a nearly constant average energy; see [17] for more details.

As shown in [18], lamellar and hexagonal phases can form within almost any simulation box (with periodic boundary conditions) that is larger than the minimum required to form a single unit cell. These phases possess at least one infinite wavelength, and can therefore orient themselves within in the simulation box so that the finite wavelengths of the pattern nearly match those of infinite, bulk, samples. For phases with *cubic* symmetry, however, the box size must be nearly a multiple of the unit cell for the cubic phase to form. Fortunately, the proper unit cell size can be estimated from the spacings of hexagonal and lamellar phases in neighboring regions of the phase diagram. We find that the unit-cell size of a body-centered-cubic micellar phase is 1.22 times the spacing between hexagonal cylinders in a neighboring region of the phase diagram. The unit-cell size of the gyroid phase is about 2.45 times the lamellar repeat period of a neighboring lamellar phase, or about 2.12 times that of a neighboring hexagonal phase. With these rules, a region of the diagram that is suspected of being able to support a cubic phase can be examined by running a simulation in a box whose size matches a multiple of the expected unit cell. For these reasons and others, boxes of various sizes and shapes are used, ranging from $20 \times 20 \times 20$ to $84 \times 84 \times 84$.

3. Results

3.1. LIQUID CRYSTALLINE PHASES IN WATER. — Figures 3a-d show (in clockwise direction) the temperature-composition phase diagram for H_4T_7, H_4T_6, H_4T_4, and H_6T_4, in water only. These phase diagrams are determined in the closed ensemble by fixing the amphiphile concentration and slowly "cooling" by increasing w in small increments, $\Delta w = 0.0038$, until an

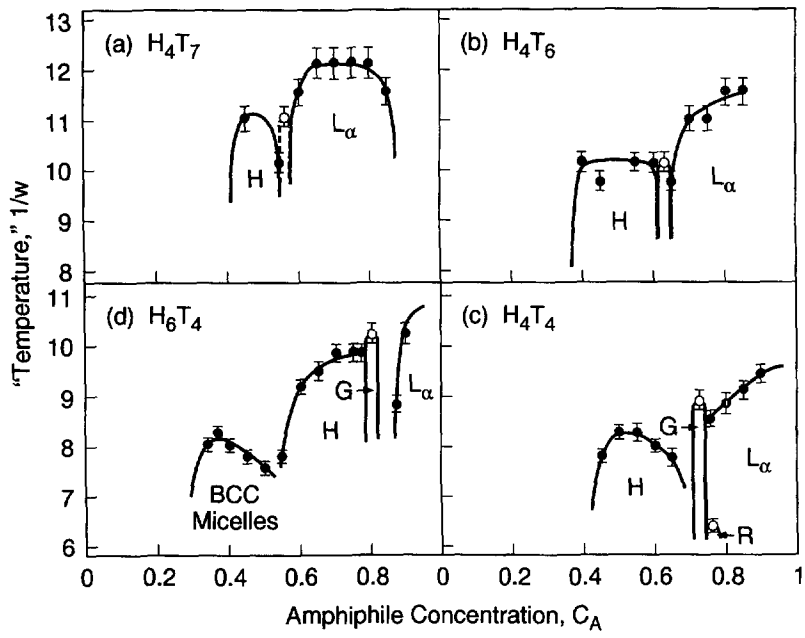

Fig. 3. — Phase diagrams of (a) H_4T_7, (b) H_4T_6, (c) H_4T_4, and (d) H_6T_4 in "water". "H" and "L_α" stand for hexagonal and lamellar, "G" and "R" are cubic gyroid and rhombohedral-like mesh intermediate phases, and "BCC micelles" is a body-centered cubic packing of spherical micelles. The closed circles are phase boundaries determined on $30 \times 30 \times 30$ lattices, while the open circles were determined on lattices of others sizes, namely $24 \times 24 \times 24$ for the gyroid phases for H_4T_4 and H_6T_4, $26 \times 26 \times 26$ for the gyroid phase for H_4T_6, $29 \times 29 \times 29$ for the gyroid phase for H_4T_7, and $34 \times 34 \times 34$ for the rhombohedral-like mesh phase for H_4T_4. The gyroid phase for H_4T_7 is marked by dashed lines, because it does not appear in every run, and may be metastable.

ordered phase appears. Runs are carried out on $30 \times 30 \times 30$ boxes, except for those producing the gyroid and rhombohedral-like phases (see below). The phases are identified by direct inspection. The transition from a disordered to an order phase is typically signaled by a drop in system energy corresponding to the loss of up to 0.1 water-tail contacts per lattice site.

Images of lamellar, cylindrical, and BCC micellar phases are shown later (see also [17,18]). A phase not reported in earlier simulations is the "gyroid", with Ia3d symmetry. For symmetric surfactants, including not only H_4T_4, but also H_3T_3 and H_6T_6, this phase appears at a concentration of $C_A = 0.73$ in water. Probably this phase forms for any symmetric amphiphile in the homologous series H_iT_i, as long as $N = 2i$ equals or exceeds 6. For symmetric surfactants, the gyroid phase appears only over a very narrow range ΔC_A of surfactant compositions, $\Delta C_A \approx 0.02$-0.03. For H_6T_6, for example, a gyroid phase forms at $C_A = 0.73$ and 0.74, but not at 0.725 or 0.745. The gyroid only appears in boxes that closely match the gyroid's preferred d-spacing; for H_6T_6, it appears for $27 \times 27 \times 27$, but not on $25 \times 25 \times 25$ nor on $29 \times 29 \times 29$ lattices. For H_3T_3 and H_4T_4, the gyroid appears for $21 \times 21 \times 21$ and $23 \times 23 \times 23$ lattices, respectively. The unit cell dimensions for H_3T_3, H_4T_4, and H_6T_6 correspond, for each surfactant, to a d spacing that is about 2.45 times the repeat spacing of the lamellar phase that forms at concentrations slightly higher than that for the gyroid phase. In each of these cases a single unit cell of the gyroid forms in the given box size. Runs with boxes large enough to contain

$2^3 = 8$ gyroid unit cells are slow to equilibrate, and have not yet produced self-assembled gyroid phases.

The structure of the gyroid phase for 73% H_6T_6 on the $27 \times 27 \times 27$ lattice is depicted in Figures 4 and 5. Figures 4a-d show slices 1, 3, 5, and 7 from this phase, while Figures 5a-d show slices 8, 10, 12, and 14. The dashed lines are the boundaries of the simulation box; the rest of the image is formed by periodic replication of the image inside the dashed lines. On slice 1 (Fig. 4a), there is a "herring-bone" pattern with two distinct tail-containing domains per unit cell; an experimental pattern similar to this can be found in an electron density map for the gyroid phase of dodecyl-trimethyl ammonium chloride (DTAC) [9]. In slice 3, (Fig. 4b), the domains are rotated slightly relative to slice 1, and in slice 5 (Fig. 4c) each domain is *connected* vertically with its two image domains in the two neighboring unit cells to form two separate zig-zag stripes per unit cell. These stripes break apart in slice 7 (Fig. 4d), leaving domains that are of similar shape and size as those in slice 1 except shifted horizontally with respect to slice 1 by half a unit cell. Figures 5a-d, representing slices 8 through 14, show a progression analogous to that of Figures 4a-d, except that in Figure 5 the domains connect (or nearly connect) in the horizontal direction; compare Figure 5c with Figure 4c. The lack of a complete connection in the horizontal direction in Figure 5c might represent an artifact of the lattice, or might be due to thermal fluctuations that are also present in real systems. Figure 5d, which represents slice 14, is similar to Figure 4a, which represents slice 1, except that in slice 14 the domains are shifted horizontally and vertically by half a unit cell. Slices 15 through 27 (not shown) just repeat the progression shown in slices 1 through 14, except with a half-unit-cell offset in both horizontal and vertical directions. Thus, the progression in slices 15 through 27 shifts the domains another half unit cell horizontally and vertically, bringing them back to the positions they occupy in slice 1.

Tracing the domains from slice to slice in Figures 4 and 5, one finds that there are *two interpenetrating, but non-intersecting*, strut networks of tail-containing units. The existence of these networks within the Ia3d symmetry group was inferred 30 years ago by Luzzati *et al.* [19, 20] in lipid/water systems; the structure they proposed for this phase is shown in Figure 6. The topology of the pair of interpenetrating networks sketched in Figure 6 is identical to that obtained in the simulations: see Figures 4 and 5. The gyroid phase has also been observed in diblock copolymer [13–15], and recently their existence in a narrow range of block-copolymer compositions between lamellar and hexagonal phases has been predicted by a self-consistent field theory [21]. Transmission electron micrograph images of the gyroid phase when viewed along the 111 axis of the Ia3d unit cell have the "wagon wheel" morphology shown in Figure 7b. This image was obtained by Thomas *et al.* [12] on a polystyrene-polyisoprene block copolymer, and the observed phase was at that time (probably incorrectly) thought to be a "double diamond" phase, which is a cubic phase closely related to the gyroid. Electron-micrograph images, such as that in Figure 7b, are obtained on samples that are many unit cells thick, and so the images are projections of the compositional pattern along the viewing direction, in this case the 111 direction. By generating such a projection along the 111 direction for the simulated gyroid phase for 73% H_6T_6, and using high contrast printing, one obtains the image shown in Figure 7a, which is similar to the experimental image in Figure 7b. Projections such as Figure 7 do not allow the gyroid phase to be clearly distinguished from the double-diamond phase. The distinction can be made in the simulations, however, by viewing the single-layer slices, such as those of Figures 4 and 5; these clearly show the topology of the strut network to be that of the gyroid phase. For experimental systems, high-order X-ray diffraction spots allow the gyroid phase to be distinguished from the double diamond [13–15].

In Figure 3, the values of w at which disorder-order transitions occur are somewhat dependent on the size of the box used in the simulations. The largest box-size effects are observed for the

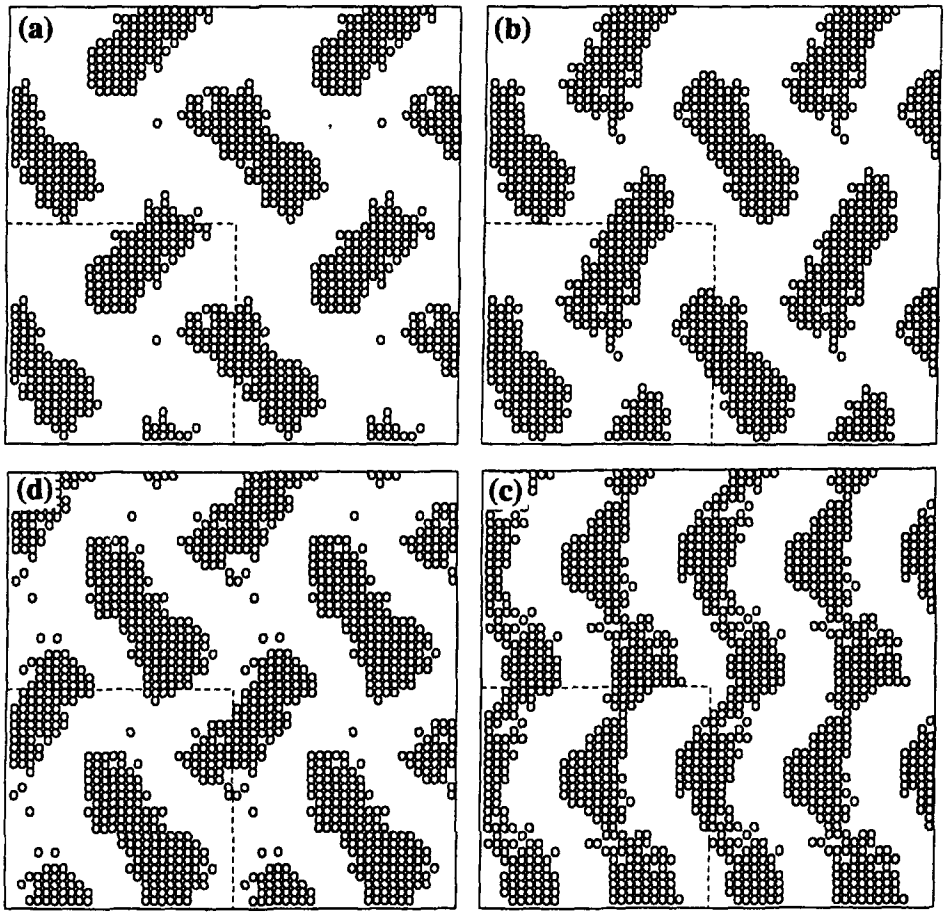

Fig. 4. — Successive parallel slices (a) 1, (b) 3, (c) 5, and (d) 7 of a gyroid structure of 73% H_6T_6 in water at $w = 0.1385$ on a $27 \times 27 \times 27$ lattice. The circles are the tail groups.

cubic micellar phases. For 50% H_6T_4, an especially large lattice-size effect occurs; an ordering transition to a micellar BCC phase is observed at $w = 0.1347$ on a $30 \times 30 \times 30$ lattice, and at $w = 0.1119$ on a $28 \times 28 \times 28$ lattice. On both lattices, eight BCC unit cells spontaneously form at the ordering transition; that is, the unit cell size is 15 on the $30 \times 30 \times 30$ lattice and 14 on the $28 \times 28 \times 28$ lattice. Boxes whose dimensions differ too much from the preferred spacing cannot support a micellar BCC phase, however. For hexagonal and lamellar phases, the effect of lattice size is much smaller; for example, for 60% H_4T_4, a hexagonal phase first forms on cooling at $w = 0.1270$ on a $30 \times 30 \times 30$ lattice, and at $w = 0.1308$ on a $40 \times 40 \times 40$ lattice. There is also hysteresis; on heating (raising w) the transition occurs at a smaller value of w than on cooling. The magnitudes of the hysteresis effects are discussed in [17]. The gyroid phase is especially sensitive to box size and only forms on boxes very close (± 1 lattice unit) to the preferred size.

Because of hysteresis and box-size effects, the phase diagrams reported in Figure 3 are semi-quantitative. Nevertheless, there are remarkable similarities between the computed phase

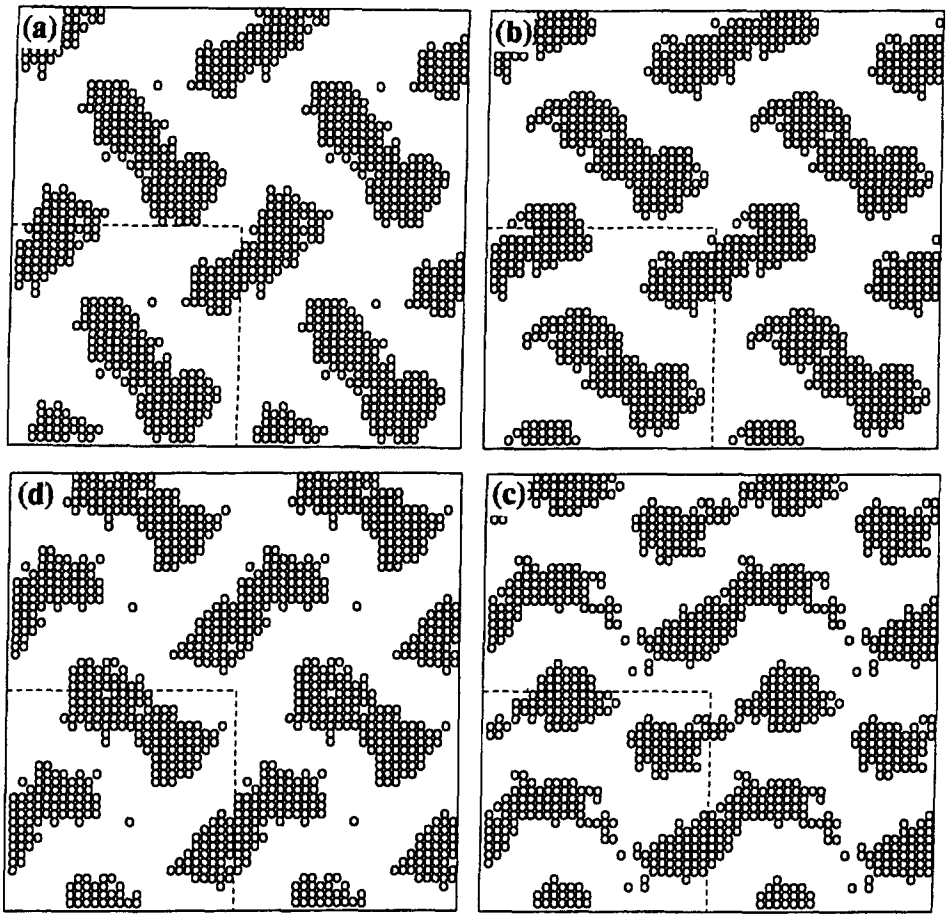

Fig. 5. — Slices (a) 8, (b) 10, (c) 12, and (d) 14 of the gyroid phase of Figure 4.

diagrams in Figure 3 and experimental ones in Figure 1. The experimentally observed phases: lamellar, gyroid, mesh, hexagonal, and micellar BCC, all occur in the simulations, and the ranges of compositions at which they appear correspond well with the experimental ranges. For a discussion and images of the simulated "mesh" tetrahedral and rhombohedral phases, see [17,18]. Note in Figure 3 that the ordering "temperature" $1/w$ is highest for the lamellar phase, and lowest for the BCC and mesh phases, in accord with the experiments. Although for H_4T_4 and H_6T_4, the transition to the gyroid phase occurs at a higher "temperature" $1/w$ than does the transition to cylinders, in disagreement with the experiments (see Fig. 1), the box size used to obtain these gyroid phases, $24 \times 24 \times 24$ for both H_4T_4 and H_6T_4, is significantly smaller than that used to obtain the cylinder phase. The smaller box, which contains only a single Ia3d unit cell, probably artificially enhances the stability of the gyroid phase, and increases the ordering transition temperature. For H_4T_6 and H_4T_7, the box sizes used to obtain the gyroid phase are larger, $26 \times 26 \times 26$ and $29 \times 29 \times 29$, respectively, and the transitions to the gyroid phase occur at lower temperatures relative to those for the hexagonal phase; see Figures 3a, b.

Figure 3 also shows that each liquid crystalline region shifts towards a higher range of

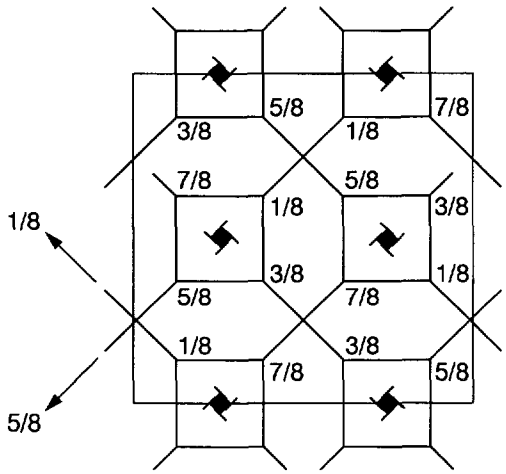

Fig. 6. — Schematic representation of the gyroid structure, which is a body-centered with space group Ia3d. The structure consists of identical finite-length rods three of which join at each junction, forming two interpenetrating three dimensional networks. The axes of the rods are represented by solid lines; the thin lines shows the unit-cell boundaries. The fractions are the z coordinates (into the page) of the structure, with the dimension of the unit cell normalized to unity (from Luzzati *et al.* [20]).

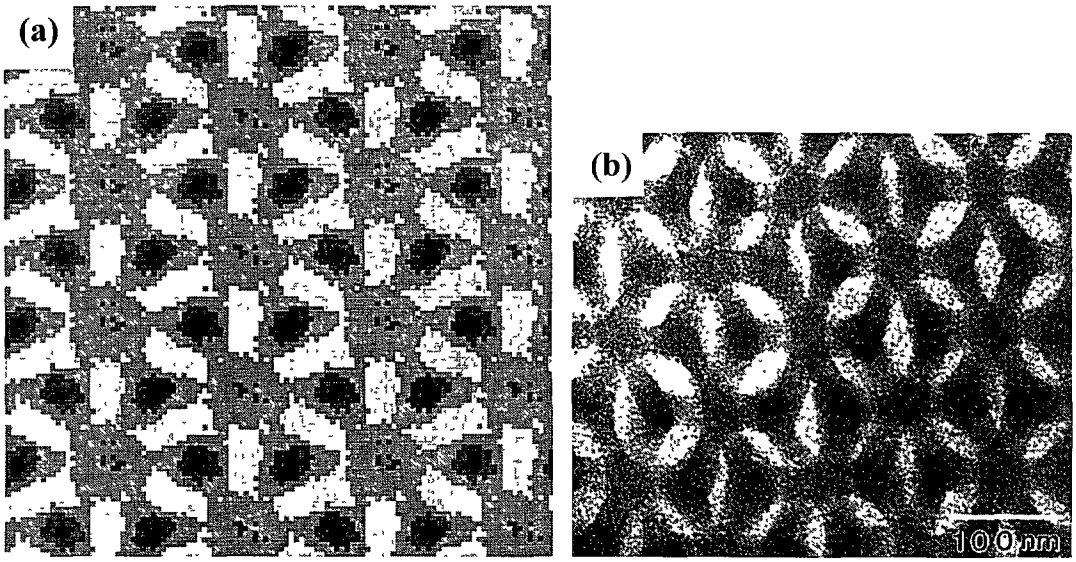

Fig. 7. — a) "Wagon wheel" image of gyroid phase formed by 73% H_6T_6 in water on a $27 \times 27 \times 27$ lattice which was periodically extended. The image was formed by projection along the 111 axis of the unit cube, using a high contrast of the tail units against the head and water units. b) Transmission electron micrograph obtained by Thomas *et al.* [12] of a cubic intermediate phase formed by a polystyrene-polyisoprene block copolymer. The phase was originally thought to be a "double diamond" phase, whose appearance in this projection is similar to that of the gyroid.

amphiphile concentrations when the ratio of the head to the tail length of the surfactant is increased from 4:7 to 6:4, in the clockwise progression from a) to d). Thus, the range of concentrations over which the hexagonal phase forms is shifted from 0.45-0.55 for H_4T_7 to 0.55-0.75 for H_6T_4. Note that for H_4T_7 the hexagonal window of compositions is rather narrow, indicating that the stability of this phase is reduced for H_4T_7. The composition range for the gyroid phase for this surfactant is marked with dashed lines (Fig. 3a), because it might be metastable. For one run on the $29 \times 29 \times 29$ lattice the gyroid phase formed, but in a repeat run at the same composition ($C_A = 0.57$), the lamellar phase formed instead. For a more asymmetric surfactant, H_4T_{10}, both the gyroid and the hexagonal phase disappear altogether, as is discussed below. Note also that the BCC phase appears for H_6T_4 in the concentration range 0.375-0.50, but does not occur at all for the other amphiphiles. Finally, at the composition $C_A = 0.50$ for both H_4T_7 and H_4T_6, the expected hexagonal phase did not form on the $30 \times 30 \times 30$ box, possibly because of an incompatibility with the box size.

The changes in phase behavior produced by the lengthening of the surfactant head group relative to the tail can be rationalized by interfacial *curvature* arguments [22–25]. Because of its longer head group, H_6T_4 prefers to reside on a curved surface with the head group on the convex side, where there is more room [22]. This favors domains with curved interfaces, such as spheres and cylinders, with tail groups packed on the inside (concave side) of the curved surfaces. Therefore, when the head group is larger, higher concentrations of surfactant are required to induce transitions to the domains with less curvature, such as transitions from spheres to cylinders or cylinders to lamellae. Since for H_6T_4 the spherical domains persist at relatively high surfactant concentrations, these domains become crowded enough to undergo an ordering transition to a cubic BCC phase. For H_4T_4, spherical domains begin to undergo transitions to elongated cigar and worm-like domains at concentrations of only around 0.35-0.40, and to hexagonal cylinders at $C_A = 0.45$, and so the spherical geometry does not persist at concentrations high enough to produce enough crowding to induce ordering of the spheres [18]. The same argument, with greater force, applies to spherical micelles of H_4T_6 and H_4T_7; these undergo transitions to oblong or cylindrical shapes at even lower surfactant concentrations. For H_4T_7, the tail group is so long that even cylinders are somewhat disfavored, and the size of the hexagonal region of the phase diagram shrinks. With still longer tail groups, as in H_4T_{10}, only lamellar phases and inverse phases can form; see below.

Comparing in more detail the phase diagrams from the simulations in Figures 3a-d to the experimental ones in Figures 1a-d, we find agreement in the general trends, but some differences in details. Generally, the compositional ranges for the hexagonal and lamellar phases, and the shifting of these ranges as one moves in the clockwise progression from a) to d) in the respective figures, have been matched reasonably well. Thus, we might infer that in the experimental diagrams, the "effective" head-to-tail size ratio increases, or, equivalently, the "packing parameter" of Israelachvili *et al.* [22] decreases, as one moves in the progression from a) to d).

The experimental diagram for an anionic surfactant, Figure 1b, shows a tetrahedral *mesh phase* at a composition of around $C_A \approx 0.75$. Elsewhere [17] it was shown that H_4T_4 forms an ordered mesh phase at this composition at a low temperature in a box of size commensurate with the preferred spacings of this phase; see Figure 3c. It would be interesting to look for mesh phase in simulations of the surfactants H_4T_7 and H_4T_6 on suitable boxes; this was not done here. C_{12} TAC has a cubic phase in the compositional window 0.45-0.55, with a biphasic cubic/disordered zone that extends down to $C_A = 0.40$. The structure of this cubic phase has apparently not been identified with certainty, although NMR diffusion studies indicate that it is a packing of spherical aggregates [26]. This window of composition agrees fairly closely with the BCC compositional range of H_6T_4, namely 0.37-0.50.

Experimental phase diagrams for surfactants related to those in Figure 1, but with larger or smaller head or tail groups, support the trends inferred from the simulations. For example, for a surfactant similar to OleGroPCho, but with a slightly shorter 16-carbon tail group, the hexagonal phase only persists down to concentrations as low as around 0.40-0.45 weight fraction [2]. Thus, a decrease in the tail length shifts the hexagonal compositional window up to higher surfactant concentrations, as expected. An extensive study by Mitchell *et al.* [27] of ethyleneglycol ethers C_iEO_j with i ranging from 8 to 16 and j from 3 to 12 gives qualitatively the expected shifts in the hexagonal and other ordered phases with changes in the lengths of head or tail groups. Not surprisingly, the cubic micellar phase only occurs when the surfactant head group is relatively large compared to the hydrocarbon tail group.

Note in Figure 1a that the phase envelopes for $C_{12}EO_6$ are somewhat "tilted;" this tilt is not present in the phase diagrams of the other surfactants, nor in those of the simulated surfactants H_4T_4 and H_6T_4. The tilt is likely due to the temperature dependence of the degree of hydration of the head groups of this nonionic surfactant. As the temperature is raised, the hydration number of the head group EO_6 decreases [27–29], making it effectively less bulky, and one would therefore expect a shift of each compositional window toward lower surfactant concentration, as observed. Notice also that this surfactant has a "re-entrant" isotropic phase; at high concentrations of surfactant, the lamellar phase disappears and is replaced, surprisingly, by a disordered phase. This is thought to be due to special interactions between EO_6 groups [27]. It is possible that rather modest extensions of the lattice model might allow these interactions to be mimicked, thus permitting the computation of more accurate phase diagrams.

Figure 8 shows the phase diagrams of surfactants with more extreme ratios of head-to-tail lengths than those of Figure 3, namely those of $H_{10}T_4$, H_4T_{10}, $H_{16}T_4$, and H_4T_{16}, and compares them to that of H_4T_4. In Figures 8b, d, and f, the diagrams for H_4T_4, H_4T_{10}, and H_4T_{16} are plotted against water concentration $(1 - C_A)$, and presented as continuations of the diagrams, respectively, for H_4T_4, $H_{10}T_4$, and $H_{16}T_4$. Because of the symmetries of the model used here, the phase diagram for H_iT_j in water is equivalent to one for the "complementary" surfactant H_jT_i in oil. Hence, if one interprets the diagrams on the right side of Figure 8 as those of the complementary surfactants in oil, then as one moves from left to right in Figures 8a-b, c-d, or e-f, the volume ratio of lyophilic to hydrophilic species increases continuously, and Figures 8a-b, 11c-d, and 11e-f can each be considered a single "extended" phase diagram. Figures 8a-b is qualitatively similar to a hypothetical phase diagram proposed by Seddon [30]. Note in Figure 8, that as one increases the asymmetry of the surfactant, there is a rightward shifting of each extended diagram, and a loss of phases on right side of the diagram. For the most asymmetric surfactant/complement, $H_{16}T_4/H_4T_{16}$, only sphere packings are formed by $H_{16}T_4$, while for H_4T_{16}, lamellar phases, and *inverse* hexagonal and *inverse* gyroid phases form, but the "normal" hexagonal phase is missing.

Thus, when the surfactant tail is very long relative to the head, the surfactant eschews normal type I spherical and cylindrical micelles and prefers *inverse* (or type II) structures, such as type II hexagonal (and gyroid) phases, in which the heads and water units are inside of the cylinders, and only tails are outside. Note also that for the surfactant with the longest tail group, H_4T_{16}, the size of the region of G_{II} phase is enlarged somewhat; it spans a compositional range of 0.055 ± 0.015 in width, compared to a width of only 0.025 ± 0.01 for more symmetric surfactants. Consistent with these findings, long-tailed monoglycerides [5,31–33] and two-tailed lipids such as phosphatidyl choline or di-dodecyl alkyl-β-D-glucopyranosyl-rac-glycerol [6] have large regions of inverse hexagonal and inverse gyroid phases; see Figure 2. However, the sizes of the gyroid II regions in the experimental phase diagrams in Figure 2 are much larger than those of the theoretical diagrams in Figures 8d, f. The experimental diagrams also possess regions of

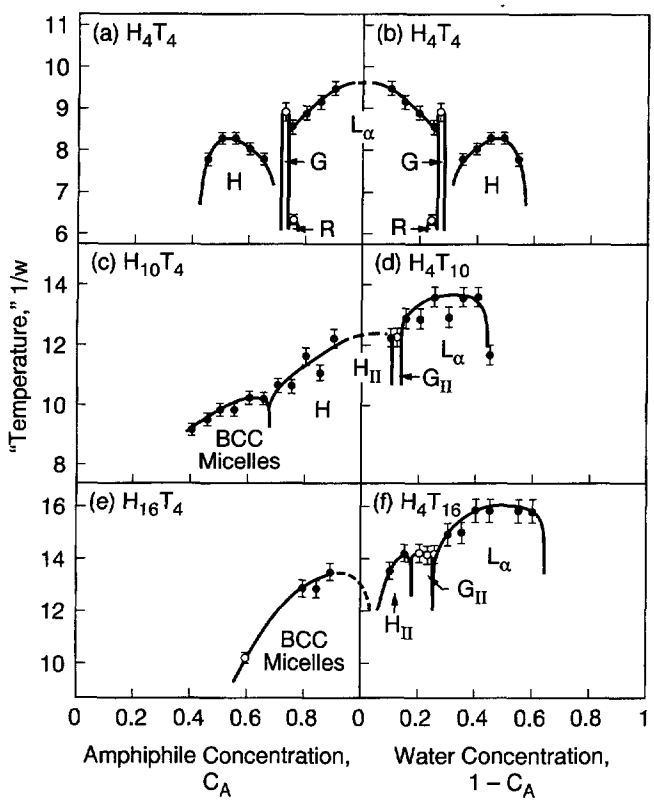

Fig. 8. — Phase diagrams of (a) H_4T_4, (c) $H_{10}T_4$, and (e) $H_{16}T_4$ plotted against surfactant concentration C_A, and those of the "complementary" surfactants (b) H_4T_4, (d) H_4T_{10}, and (f) H_4T_{16}, plotted against water concentration, $1 - C_A$. The symbols mean the same as in Figure 3. Because of the symmetry of the model, the diagrams for H_4T_4, H_4T_{10} and H_4T_{16} in water are equivalent to those of the complementary surfactants H_4T_4, $H_{10}T_4$, and $H_{16}T_4$ in oil. The closed circles are phase boundaries determined on $30 \times 30 \times 30$ lattices, while the open circles were determined on lattices of others sizes, namely $24 \times 24 \times 24$ for the gyroid phase and $34 \times 34 \times 34$ for the rhombohedral-like mesh phase of H_4T_4; $28 \times 28 \times 28$ for the inverse gyroid phase of H_4T_{10}; $33 \times 33 \times 33$ for the BCC phase ($C_A = 0.60$) of $H_{16}T_4$; and $34 \times 34 \times 34$ for the inverse gyroid and lamellar phases ($C_A = 0.80$) of H_4T_{16}.

"double diamond" D_{II} phase that have not yet been found in the simulations. The conditions under which the double-diamond phase might appear instead of the gyroid phase have been discussed by Hyde [25]. In addition, the experimental diagrams (Fig. 2) are dominated by thermotropic order-order transitions not evident in the simulations. Larsson [5] argues that increasing temperature or increasing water content tends to increase the hydrocarbon chain disorder in these lipids, which brings about the observed thermotropic phase transitions. These, and other causes for the thermotropic character of the phase transition, and the greatly enlarged regions of bicontinuous cubic phase in one- and two-tailed lipids, are not captured by the model surfactants considered here.

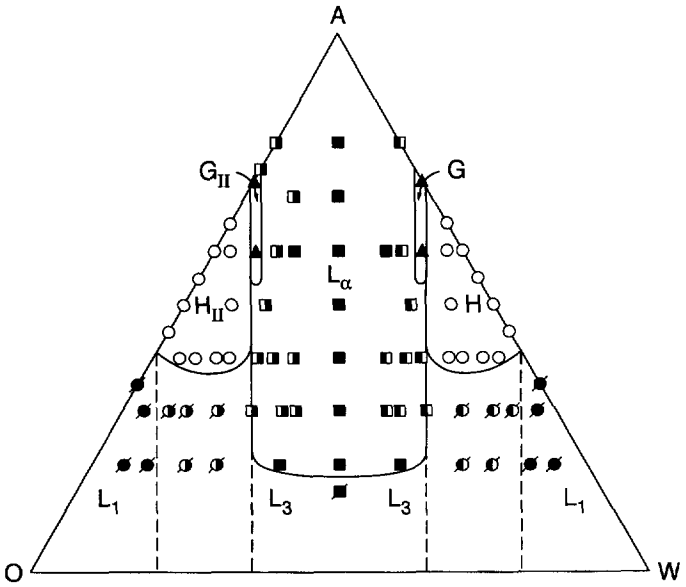

Fig. 9. — Ternary phase diagram for H_4T_4 in oil and water at $w = 0.1538$ ($Nzw = 32$). "L_1" is a disordered micellar phase with (●) representing spherical micelles and (◑) oblong micelles; "L_3" (■) is a disordered bicontinuous phase, "H" (○) a hexagonal cylindrical phase, "G" (▲) a gyroid cubic intermediate phase, and "L_α" a lamellar phase, with (■) representing lamellae without holes, (◨) representing lamellae with holes in the aqueous layers, and (◧) representing lamellae with holes in the oleic layers. The dashed lines represent, from left to right, the fixed hydrophilic compositions, $C_H = 0.20$, 0.35, 0.65, and 0.80.

3.2. Liquid Crystalline Phases in Water and Oil. — Figure 9 shows the surfactant-oil-water ternary phase diagram for H_4T_4 at $w = 0.1538$, which corresponds to $Nzw = 32$; the symbols are defined in the caption. This phase diagram was obtained by a combination of simulations in partially open and in closed ensembles. Only one half of the phase diagram for H_4T_4 was simulated; the other half was obtained by symmetry. The box sizes used to obtain these results are summarized in Table I.

In Figure 9, the *lamellar* phase occupies the central part of the phase diagram, flanked by regions of *hexagonally* packed cylinders. Sandwiched between the cylindrical and lamellar regions are slender zones occupied by regular and inverse the *gyroid* phases, G and G_{II}. Since there are multiple chemical components, there should be multi-phase coexistence regions between the various liquid crystalline phases in Figure 9. But these regions cannot be determined except with simulations with very large boxes, or with simulations with fully open ensembles, in which the surfactant concentration, as well as the oil/water ratio, can vary. We believe that the coexistence regions are small.

The half-closed squares in Figure 9 denote lamellae with *holes*, or perforations. These perforated lamellae occur at asymmetric compositions — that is, lamellae whose compositions are near the phase boundaries on either side of the lamellar zone. For lamellae on the water-rich side of the diagram, the holes are in the lamellae that contain oil (and tails), while on the oil-rich side, the holes are in the lamellae that contain water (and heads). Images of these perforated lamellae have been presented earlier [17]. The perforations allow the lamellae to accommodate unequal amounts of oil and water without changing their spacings much; a large

Table I. — *Lattice sizes in simulations of ternary phase diagrams.*

Surfactant	Concentration	Box Sizes
H_4T_4	0.80	$20 \times 20 \times 20$, $40 \times 40 \times 40$
H_7T_4	0.75	$30 \times 30 \times 30$
H_4T_4	0.70	$30 \times 30 \times 30$
H_4T_4	0.60	$30 \times 30 \times 30$
H_7T_4	0.60	$30 \times 30 \times 30$
H_4T_4	0.50	$30 \times 30 \times 30$
H_7T_4	0.45	$30 \times 30 \times 30$
H_4T_4	0.40	$30 \times 30 \times 30$
H_7T_4	0.35	$35 \times 35 \times 35$
H_4T_4	0.30	$40 \times 40 \times 40$
H_7T_4	0.25	$40 \times 40 \times 40$
H_4T_4	0.20	$40 \times 40 \times 40$, $35 \times 35 \times 35$
H_7T_4	0.15	$45 \times 45 \times 45$

spacing change would be disfavored because it would force the tail or head groups to change significantly their configurations. When lamellae containing holes are cooled, the holes can organize onto a lattice with hexagonal or tetragonal order [17,18]. For H_4T_4, hexagonal ordering occurs at $w = 0.1614$; see Figure 3. Since this value of w is greater than that at which Figure 9 was determined, lamellar phases with ordered holes are not present in the phase diagram of Figure 9.

The dashed lines in Figure 9 correspond to fixed concentrations C_H of hydrophilic units (water and heads). The left-most dashed line corresponding to $C_H = 0.20$ marks the concentration above which the hexagonal phase appears. The dashed line at $C_H = 0.35$ separates the oil-rich hexagonal (H_{II}) from the oil-rich gyroid (G_{II}) or the lamellar phase; the dashed line at $C_H = 0.65$ separates the lamellar phase from the water-rich gyroid or hexagonal phase, and the line at $C_H = 0.80$ is the boundary beyond which there are no more ordered phases. Note that the phase boundaries closely follow these straight lines. Thus, *the order-order phase transitions in the* H_4T_4 *system occur at fixed values of the total concentration of hydrophilic units.*

The phase diagram in Figure 9 is symmetric about an oil/water ratio of unity because of the head/tail symmetry of H_4T_4 and the perfect symmetry of the interaction energies. Real amphiphilic solutions are never perfectly symmetric. As a preliminary step exploring the role of asymmetry, we determine the phase diagram for an asymmetric amphiphile H_7T_4 at $w = 0.1119$; see Figure 10. This value of w for H_7T_4 corresponds to the same value of Nzw ($Nzw = 32$) as that for H_4T_4 at $w = 0.1538$. Note in Figure 10 the presence of hexagonal and lamellar phases, just as for H_4T_4. The phase diagram for H_7T_4 is strongly *asymmetric*, however; a very large region of hexagonal phase is found on the water-rich side of the diagram, but only a small one on the oil-rich side. In addition, only the water-rich side shows a BCC phase of spherical micelles, which is absent entirely from the phase diagram of H_4T_4. The dashed lines in Figure 10 correspond to same fixed values of the hydrophilic concentrations C_H as in Figure 9: namely, $C_H = 0.20$, 0.35, 0.65, and 0.80, from left to right. Relative to these,

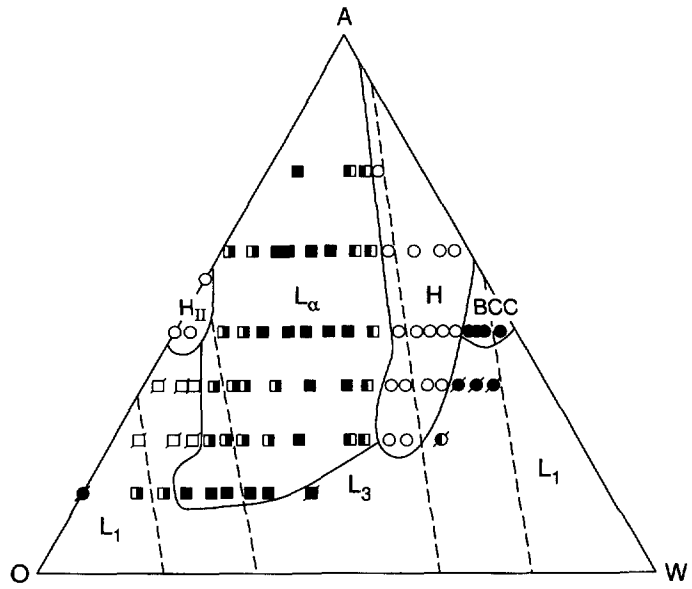

Fig. 10. — Ternary phase diagram for H_7T_4 in oil and water at $w = 0.1119$ ($Nzw = 32$). The symbols and lines are as in Figure 9; with (□) representing lamellae with oblong holes or "stripes".

the regions of ordered phases for H_7T_4 are all *shifted to the left*, especially at low surfactant concentration. These trends in the phase behavior of H_7T_4 mixed with oil and water can be qualitatively explained by curvature arguments, similar to those discussed in Section 3.2.

Simulations of H_7T_4 at compositions near the left side of the lamellar boundary in Figure 10 at surfactant concentrations in the range $C_A = 0.15$-0.35 show anomalous, highly hysteretic, behavior. Consider a water/oil ratio corresponding to a lamellar phase with holes near the left boundary of the lamellar phase in Figure 10. If the chemical potential $\Delta\mu$ is lowered so that C_W decreases, and the boundary on the left side of the lamellar phase in Figure 10 is crossed, the lamellar phase with holes persists, but the holes increase in size *anisotropically*, becoming highly oblong in shape, the more so as $\Delta\mu$ continues to decrease and C_W gets still smaller. Figures 11a-c show slices through the mid-planes of the head-and-water-containing lamellar layers of 25% H_7T_4 at (a) $\Delta\mu = -0.25$, where $C_W = 0.1742$, at (b) $\Delta\mu = -0.35$, where $C_W = 0.135$, and at (c) $\Delta\mu = -0.85$, where $C_W = 0.060$. A transition from irregularly sized circular holes to stripe-shaped holes occurs as the water concentration diminishes.

A transition from circular holes to stripes was predicted recently by Bagdassarian *et al.* [34] using an analytic "defect model". In our simulations, the stability of the "stripe phase" is uncertain. When a simulation starts from a completely disordered state at $w = 0$, and w is slowly incremented to $w = 0.1119$, holding the chemical potential fixed at $\Delta\mu = -0.35$, the "stripe phase" is not obtained, only a disordered state with no clear lamellar order. Thus although the "stripe phase" persists during long simulation runs, it may nevertheless be only a metastable phase. (Within the area marked "L_α" in Figs. 9 and 10, lamellar phases, with or without holes, are obtained from the disordered state by slow cooling, confirming that the lamellar phases within this region are thermodynamically stable.) The "stripe phase" is indicated by the symbols (□) in Figure 10, which are left outside the boundary of the L_α region, because of the uncertain thermodynamic status of this phase.

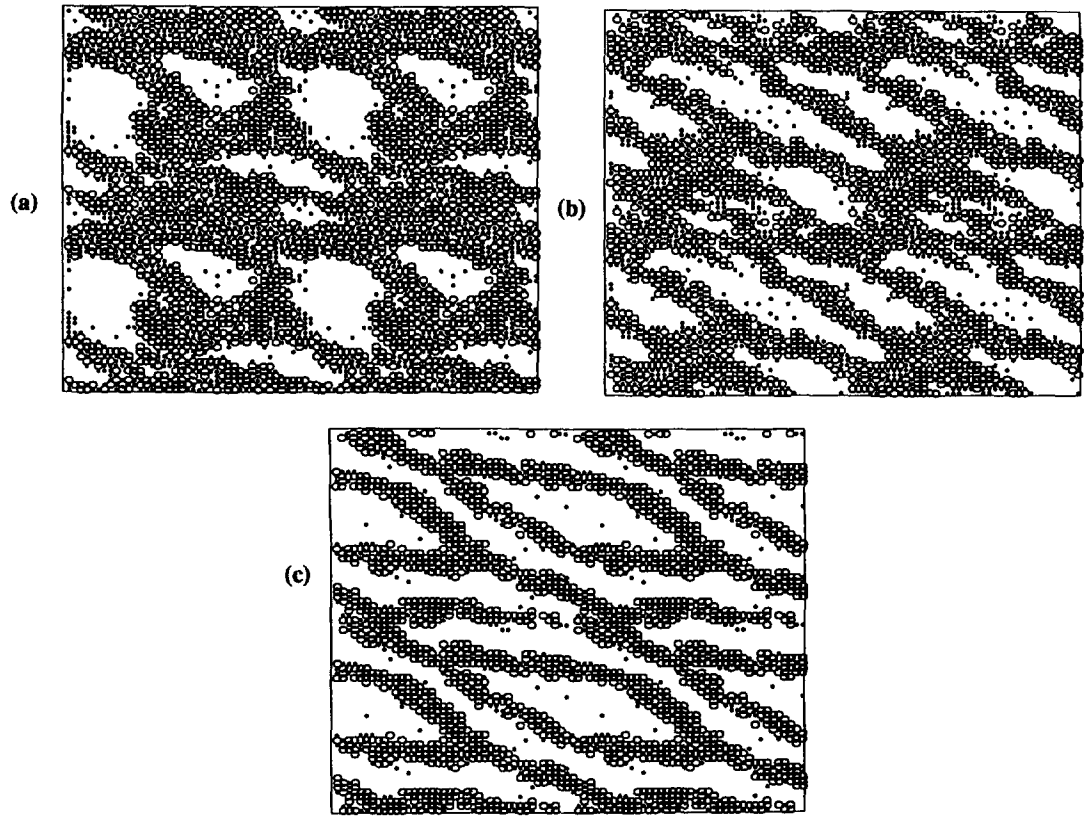

Fig. 11. — Slices through the mid-plane of the head-and-water lamellar layers of 25% H_7T_4 at $w = 0.1119$ and (a) $\Delta\mu = -0.25$, $C_W = 0.174$; (b) $\Delta\mu = -0.35$, $C_W = 0.135$; and (c) $\Delta\mu = -0.85$, $C_W = 0.060$. The circles are head units and the asterisks are water units.

Since the "stripe" phase is completely absent from the phase diagram of H_4T_4, its presence (whether stable or metastable) in the ternary diagram for H_7T_4, must be a manifestation of head/tail asymmetry. Curvature concepts suggest that H_7T_4 systems are reluctant to undergo a transition from lamellar to a type II cylinder phase even when the volume of hydrophilic material no longer suffices to support an ordinary lamellar phase. The stripe phase may emerge as the byproduct of this "frustration".

Figures 12a, b are plots of the oil/water ratio *versus* the chemical potential difference $\Delta\mu$ for H_4T_4 and H_7T_4 at various surfactant concentrations. The lower the concentration of surfactant, the more rapidly the oil/water ratio changes with $\Delta\mu$. Small discontinuities are evident at transitions between lamellar and hexagonal phases, for H_4T_4 at $C_A = 0.5$ and 0.4.

3.3. EPITAXIAL RELATIONSHIPS. — As the water concentration is increased for H_7T_4 at $C_A = 0.45$, there is a phase transition from the hexagonal cylindrical phase to the BCC spherical phase; see Figure 10. Figure 13 shows slices of a system containing 45% H_7T_4 at various water concentrations. These slices are parallel to the plane defined by an edge and a face diagonal of the $30 \times 30 \times 30$ lattice; in this orientation, the slices are parallel to the hexagonal cylinders at $\Delta\mu = 0.2$, $C_O = 0.127$; see Figure 13a. The cylinders in Figure 13a are well defined, and rather uniformly thick, oriented along the *body diagonal* of the lattice. At

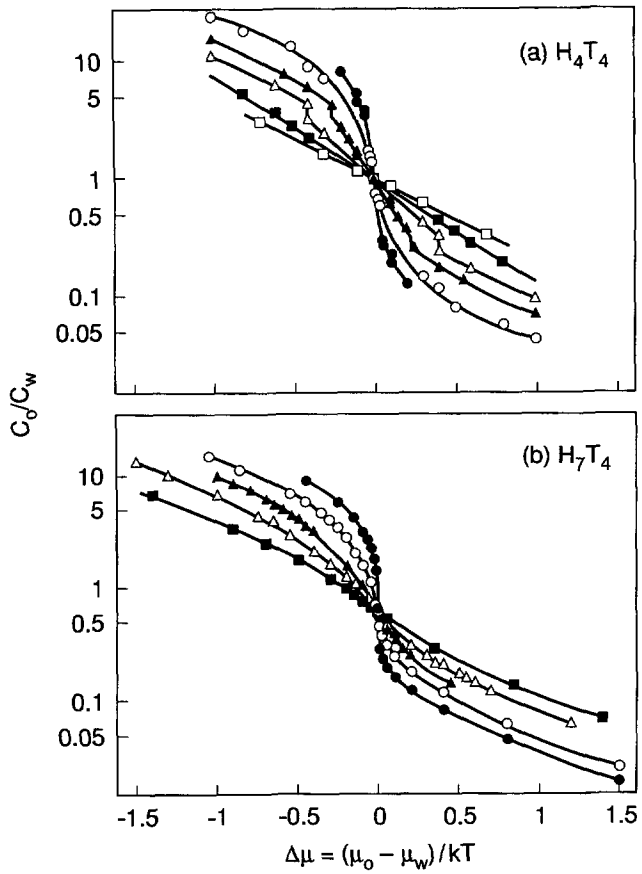

Fig. 12. — The ratio of volume fractions of oil to water *versus* chemical potential difference $\Delta\mu \equiv (\mu_0 - \mu_w)/k_BT$ at various surfactant concentrations C_A for (a) H_4T_4 at $C_A = 0.2$, 0.3, 0.4, 0.5, 0.6, and 0.7; and (b) H_7T_4 at $C_A = 0.15$, 0.25, 0.35, 0.45, and 0.60. The steepness of the curves increase monotonically with decreasing surfactant concentration.

$\Delta\mu = 0.4$, $C_O = 0.093$ (Fig. 13b), the cylinders become nonuniform in thickness, apparently due to pre-transitional fluctuations. At $\Delta\mu = 0.55$, $C_O = 0.072$ (Fig. 13c), the cylinders break apart into irregular fragments. Finally, at $\Delta\mu = 0.7$, $C_O = 0.059$ (Fig. 13d), the fragments become fairly uniform in size and assemble onto a BCC lattice, with the 111 direction corresponding to the orientation of the precursor hexagonal cylinders. This epitaxial relationship between the orientation of the cylinders and that of the unit cell of the BCC cubic phase has been observed experimentally in thermotropic block copolymer systems by Koppi *et al.* [35]. It implies that the unit cell dimension of the BCC cubic phase is $\sqrt{6}/2 = 1.22$ times that of the hexagonal phase. *A priori*, one might imagine that the transition from hexagonal cylinders to BCC spheres might occur by way of regular undulations that pinch off to form the spheres [35]. However, in the simulations, the transition from hexagonal cylinders to BCC spheres involves instead a rathered disordered intermediate state; see Figure 13c.

Epitaxial relationships also exist among the gyroid, lamellar, and hexagonal phases. To explore these, a gyroid phase was prepared by slowly "cooling" to $w = 0.1231$ a mixture of

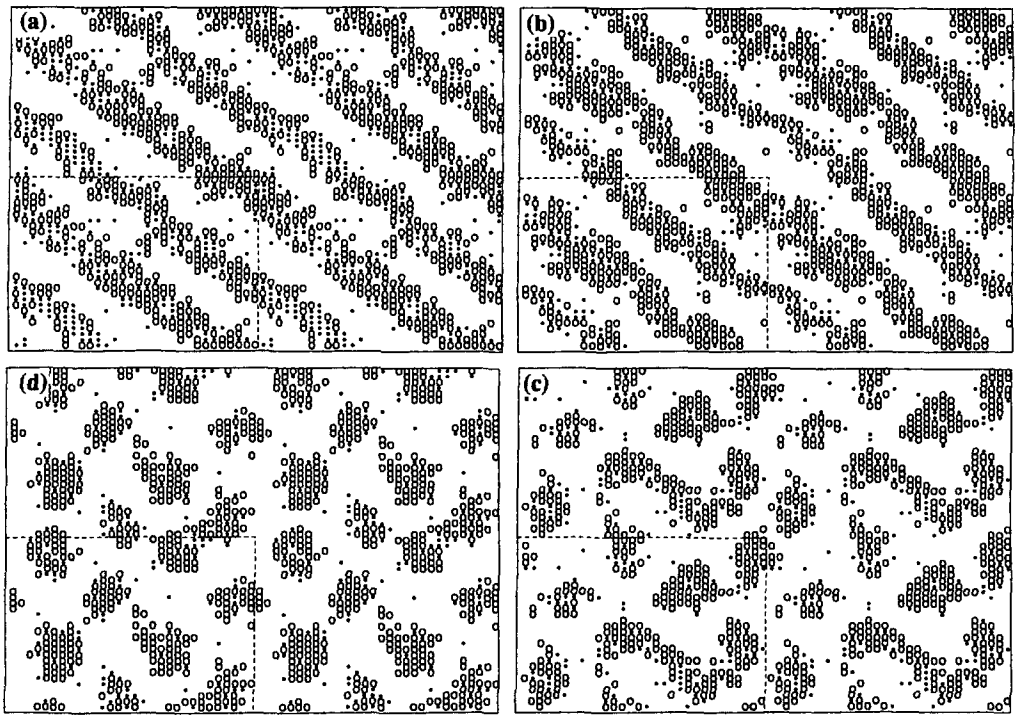

Fig. 13. — Slices parallel to a face diagonal and an edge of 30 × 30 × 30 lattices, for 45% H_7T_4 at $w = 0.1119$. This slice is in the plane of the hexagonally packed cylinders in a), which are oriented along the body diagonal of the lattice. (a) $\Delta\mu = 0.2$, $C_O = 0.127$; (b) $\Delta\mu = 0.4$, $C_O = 0.093$; (c) $\Delta\mu = 0.55$, $C_O = 0.072$; and (d) at $\Delta\mu = 0.7$, $C_O = 0.059$. The circles are the tail groups, and the asterisks are oil units.

60% H_4T_4 and 6.5% oil on a 24 × 24 × 24 lattice in the closed ensemble. The ensemble was then changed to the partially open one with $\Delta\mu = 0.8$, at which the oil concentration remained at around 6.5%. In the partially open ensemble, $\Delta\mu$ was then increased in small steps until the gyroid phase transformed to a hexagonal phase at $\Delta\mu \approx 1.5$, $C_O = 0.03$. Starting again with the gyroid phase at $\Delta\mu = 0.8$, and decreasing $\Delta\mu$ in small steps, a transition to a lamellar state with holes was observed at $\Delta\mu \approx 0.4$, $C_O = 0.125$. Two mutually orthogonal slices (parallel to two different faces of the simulation box) of these hexagonal and lamellar phases formed by transitions from the gyroid phase are shown in Figures 14 and 15. The hexagonal and lamellar spacings are 11.3 and 9.8, respectively. The ratios of the d spacings of lamellar:hexagonal:gyroid phases are $1{:}2/\sqrt{3}{:}\sqrt{6} = 1{:}1.15{:}2.45$, which is very similar to the epitaxial ratios predicted by mean-field theory, and observed experimentally, for these phases in block copolymers [36]. Figure 16 shows a single slice parallel to a face of the 24 × 24 × 24 lattice in the a) hexagonal, b, c) gyroid, and d) lamellar phases, produced at different values of $\Delta\mu$. The cylinders in Figure 14 are oriented along a diagonal of the 24 × 24 × 24 box; thus, a 111 direction of the gyroid phase is parallel to the cylinder orientation in the hexagonal phase; this finding that agrees with experimental observations of gyroid-to-hexagonal transitions for $C_{12}EO_6$ and other surfactants [4, 9, 37, 38], and for block copolymers [13, 14]. Likewise, the

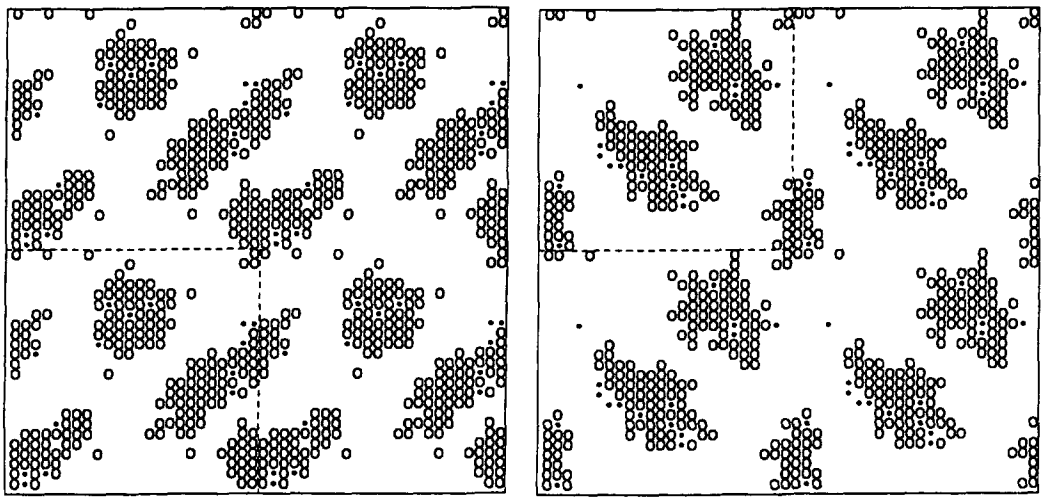

Fig. 14. — Two mutually orthogonal slices through the hexagonal phase for 60% H_4T_4 at $w = 0.1231$, $\Delta\mu = 1.5$, on a $24 \times 24 \times 24$ lattice. The circles are the tail groups, and the asterisks are oil units. In this and following figures, the slices are all parallel to a face of the simulation box.

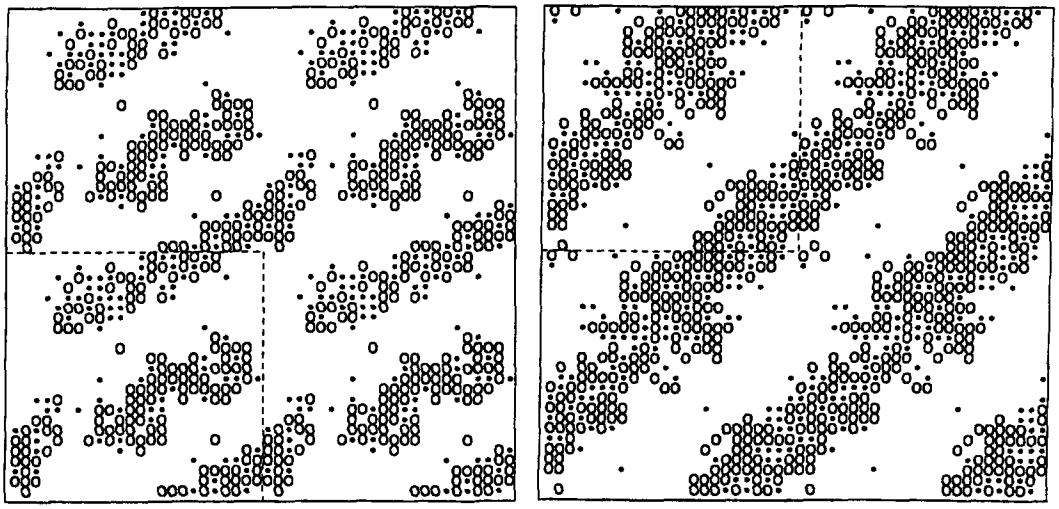

Fig. 15. — Two mutually orthogonal slices through the lamellar phase for the system described in Figure 14 with $\Delta\mu = 0.4$.

epitaxial relationship (001) $\longleftrightarrow$ (211) between unit-cell orientations of the gyroid and the lamellar phases shown in Figure 15 is consistent with experimental findings [38]. A similar transition with the same epitaxial relationships among the phases occurs when 77% H_4T_{16} in water is cooled from $w = 0.0723$ (H_{II} phase) to $w = 0.0741$ (G_{II} phase) to $w = 0.0759$ (lamellar phase) on a $32 \times 32 \times 32$ lattice. Thus, the epitaxial relationships among these phases appear to be universal. Although we have not yet made a detailed study of the transitional pathways

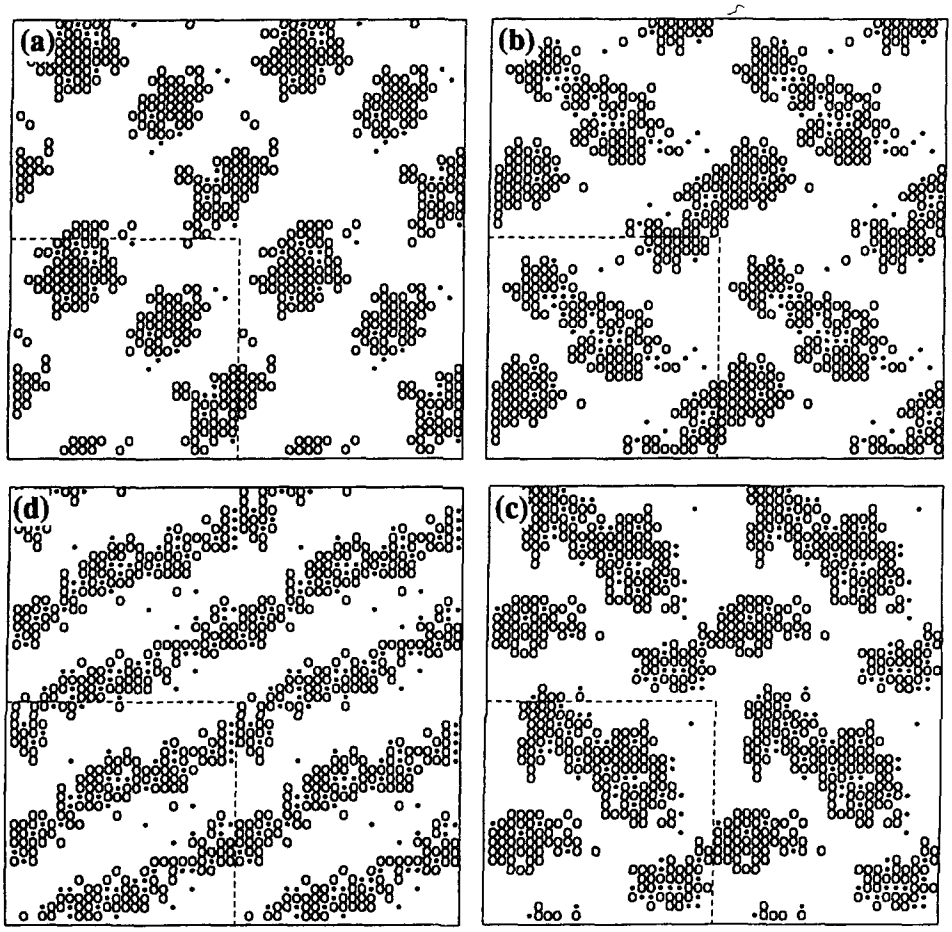

Fig. 16. — A slice parallel to a face of the 24 × 24 × 24 lattice containing 60% H_4T_4 at $w = 0.1231$, described in Figure 14, and (a) $\Delta\mu = 1.5$, $C_O = 0.03$ (hexagonal); (b) $\Delta\mu = 0.9$, $C_O = 0.061$ (gyroid); (c) $\Delta\mu = 0.6$, $C_O = 0.089$ (gyroid); and (d) $\Delta\mu = 0.4$, $C_O = 0.125$ (lamellar). The circles are the tail groups, and the asterisks are oil units.

from one phase to another, preliminary observations indicate that the transition to lamellae involves a rather disordered transitional state.

4. Final Comments

The simple lattice model for surfactant-oil-water mixtures explored here mimics remarkably well the *binary* phase behavior of several experimental surfactant systems in which the head-to-tail size ratios are not extreme. This suggests that the phase behavior of these surfactants is dominated by physical phenomena that are captured by the lattice model, including volume-filling constraints, the ratio of "effective" head to tail sizes, the configurational entropy of the surfactant chain, and the repulsive interactions between hydrophilic and hydrophobic moieties. The differences in physico-chemical details among various surfactants can to a significant

degree be accounted for by allowing for differences in ratios of effective sizes of head to tail groups. The agreement between simulation and experiment may seem surprising; while the hydrocarbon or fluorocarbon surfactant tail is modeled with some degree of realism, the lattice treatment of the water and head groups, and their interactions with each other, would seem to be hopelessly crude. Nevertheless, the good correspondence between predicted and experimental phase diagrams suggests that the complex interactions of the real system can to a remarkable degree be mapped onto a simplistic model, and that the phase behavior of many systems is controlled mostly by rather gross features, such as an effective head group area or volume, and effective interaction energies. The similar phase progressions observed in surfactant phase diagrams and those recently predicted for mixtures of A-B diblock and A homopolymers reinforces the conclusion that these features of amphiphilic phase diagrams are universal [39].

The lattice model works much less well in explaining the behavior of lipids, which have especially bulky single or double tails [5,6]. As mentioned above, the phase behavior of these is dominated by inverse phases, including multiple inverse cubic phases, such as the inverse Ia3d gyroid phase, the inverse Pn3m "double-diamond" phase, as well as an inverse hexagonal phase. Other two-tailed surfactants when mixed with water and hydrocarbon, have as many as five distinct bicontinuous cubic intermediate phases phases [40]. It would be interesting to see if these characteristics could be predicted from simple lattice or off-lattice [41] models of two-tailed surfactants.

The good correspondence between experimental and simulated binary phase diagrams (Figs. 1 and 3) for not-too-asymmetric surfactants is not matched in the phase diagrams of *ternary* surfactant-oil-water mixtures. The simulated diagrams (Figs. 9 and 10) do not bear much resemblance to experimental ones, which are dominated by large multiphase regions [42–44]. It is possible that the simulations would show large multiphase regions if the lattice sizes were larger. However, it is perhaps more likely that the single-site representation of "oil" molecules in the simulations is too extreme a divergence from reality to permit even qualitative comparisons to be made to the phase behavior when oil is present. A more fitting experimental system with which to compare the simulations might be a short-chain A-B diblock copolymer mixed with monomers or short oligomers of A and B.

References

[1] Balmbra R.R., Clunie J.R. and Goodman J.F., *Nature* **222** (1969) 1159-1160.
[2] Arvidson G., Brentel I., Khan A., Lindblom G. and Fontell K., *Eur. J. Biochem.* **152** (1985) 753-759.
[3] Kekicheff P. and Tiddy G.J.T., *J. Phys. Chem.* **93** (1989) 2520-2526.
[4] Clerc M., Levelut A.M. and Sadoc J.F., *J. Phys. Colloq. France* **51** (1990) C7-97-C7-104.
[5] Larsson K., *J. Phys. Chem.* **93** (1989) 7304-7314.
[6] Turner D.C., Wang Z.-G., Gruner S.M., Mannock D.A. and McElhaney R.N., *J. Phys. II France* **2** (1992) 2039-2063.
[7] Eriksson P.O., Lindblom G. and Arvidson G., *J. Phys. Chem.* **91** (1987) 846-853.
[8] Blackburn J.C. and Kilpatrick P.K., *J. Coll. Inter. Sci.* **149** (1992) 450-471.
[9] Mariani P., Amaral L.Q., Saturni L. and Delacroix H., *J. Phys. II France* **4** (1994) 1393-1416.

[10] Hasegawa H., Tanaka H., Yamasaki K. and Hashimoto T., *Macromolecules* **20** (1987) 1651-1671.
[11] Winey K.I., Thomas E.L. and Fetters L.J. *Macromolecules* **25** (1992) 2645-2650
[12] Thomas E.L., Anderson D.M., Henkee C.S. and Hoffman D., *Nature* **334** (1988) 598-601.
[13] Förster S., Khandpur A.K., Zhao J., Bates F.S., Hamley I.W., Ryan A.J. and Bras W., *Macromolecules* **27** (1994) 6922-6935.
[14] Hadjuk D.A., Harper P.E., Gruner S.M., Honeker C.C., Kim G., Thomas E.L. and Fetters L.J. *Macromolecules* **27** (1994) 4063-4075.
[15] Hadjuk D.A., Harper P.E., Gruner S.M., Honekar C.C., Thomas E.L. and Fetters L.J. *Macromolecules* **28** (1995) 2570-2573.
[16] Larson R.G., *J. Chem. Phys.* **83** (1984) 2411-2420; *ibid.* **87** (1988) 1642-1650.
[17] Larson R.G., *J. Chem. Phys.* **92** (1992) 7904-7918.
[18] Larson R.G., *Chem. Eng. Sci.* **49** (1994) 2833-2850.
[19] Luzzati V. and Spegt P.A., *Nature* **215** (1967) 701-704.
[20] Luzzati V., Tardieu A., Gulik-Krzywicki T., Rivas E. and Reiss-Husson R. *Nature* **220** (1968) 485-488.
[21] Matsen M.W. and Schick M., *Phys. Rev. Lett.* **72** (1994) 2660-2663.
[22] Israelachvili J., Mitchell D.J. and Ninham B.W., *J. Chem. Soc. Faraday Trans. I* **72** (1976) 1525-1568.
[23] Helfrich W., *J. Phys. France* **48** (1987) 291-295.
[24] Sadoc J.F. and Charvolin J., *J. Phys. France* **47** (1986) 683-691.
[25] Hyde S.T., *J. Phys. Colloq. France* **51** (1990) C7-209-C7-228.
[26] Fontell K., *Mol. Cryst. Liq. Cryst.* **63** (1981) 59-82.
[27] Mitchell D.J., Tiddy G.J.T., Waring L., Bostock T. and McDonald M.P., *J. Chem. Soc. Far. Trans. I* **79** (1983) 975-1000.
[28] Nilsson P.G. and Lindman B., *J. Phys. Chem.* **87** (1983) 4756-4761.
[29] Puvvada S. and Blankschtein D., *J. Chem. Phys.* **92** (1990) 3710-3724.
[30] Seddon J.M., *Biochim. Biophys.* **1031** (1990) 1-69.
[31] Hyde S.T., Andersson S., Ericsson B. and Larsson K., *Z. Krist.* **168** (1984) 213-219.
[32] Lutton E.S., *J. Amer. Oil Chem. Soc.* **42** (1965) 1068-1070.
[33] Fontell K., *Coll. Polym. Sci.* **268** (1990) 264-285.
[34] Bagdassarian C.K., Roux D., Ben-Shaul A. and Gelbart W.M., *J. Chem. Phys.* **94** (1991) 3030-3041.
[35] Koppi K.A., Tirrell M., Bates F.S., Almdal K. and Mortensen K., *J. Rheol.* **38** (1994) 999-1027.
[36] Matsen M.W. and Schick M., *Macromolecules* **27** (1994) 6761-6767.
[37] Rancon Y. and Charvolin J., *J. Phys. Chem.* **92** (1988) 2646-1073.
[38] Clerc M., Levelut A.M. and Sadoc J.F., *J. Phys. II France* **1** (1991) 1263-1276.
[39] Matsen M.W., *Macromolecules* **28** (1995) 5765-5773.
[40] Ström P. and Anderson D.M., *Langmuir* **8** (1992) 691-709.
[41] Karaborni S., Esselink K., Hilbers P.A.J., Smit B., Karthäuser J., van Os N.M. and Zana R., *Science* **266** (1994) 254-256.
[42] Barnes I.S., Derian P.-J., Hyde S.T., Ninham B.W. and Zemb T.N., *J. Phys. France* **51** (1990) 2605-2628.
[43] Barois P., Eidam D. and Hyde S.T., *J. Phys. Colloq. France* **51** (1990) C7-25-C7-34.
[44] Kilpatrick P.K. and Bogard M.A., *Langmuir* **4** (1988) 790-796.